

## Infrared Optical Properties of $\text{Li}^7\text{F}$ and Natural $\text{LiF}$ at Various Temperatures, Calculated with Shell-Model Lattice-Dynamical Data\*

J. E. Eldridge and Roger Howard

*Department of Physics, The University of British Columbia, Vancouver, British Columbia, Canada*

(Received 26 October 1972)

The infrared optical properties of  $\text{Li}^7\text{F}$ , including the real and imaginary dielectric constants, the extinction and absorption coefficient, the refractive index, conductivity, reflectivity, and phase angle, have been calculated absolutely, assuming two-phonon "summation" or "difference" relaxation of the transverse optic (TO) resonance with near-zero wave vector. A shell model, fitted to inelastic-neutron-scattering data from  $\text{Li}^7\text{F}$  at 298 °K, was used to generate the lattice-dynamical data with a density of 256 000 points per zone. The form of the potential derivatives used in the cubic-anharmonic-coupling coefficient took into account, in an approximate fashion, the long-range Coulombic coupling between other-than-nearest neighbors. The calculated constants were then compared with various experimental data, including both direct-transmission-absorption measurements and reflectivity-analysis data. The agreement in intensity and structure is generally very good, and two-phonon assignments have been made of the features in the calculated spectra. It is thought that the result of the approximation made in the cubic coupling coefficient is an overaccentuation of these features. At room temperature, there is further evidence for the need to include at least three-phonon relaxation terms, arising from quartic anharmonicity, both underneath the main resonance and above the two-phonon energy limit. At 7.5 °K the discrepancy in the width and peak height of the TO resonance between the calculated spectra, strictly applicable only to  $\text{Li}^7\text{F}$ , and the experimental data, obtained primarily from natural  $\text{LiF}$  crystals containing 7.5 at.% of the  $\text{Li}^6$  isotope, is very large. This extreme behavior is due to the fact that two-phonon relaxation of the TO resonance is almost entirely through "difference" processes, which disappear as 0 °K is approached. The damping due to the isotope-induced one-phonon processes has therefore been calculated, using once again the 298 °K shell-model data, and added to the two-phonon damping. The absorption coefficient, refractive index, and reflectivity were then calculated for natural  $\text{LiF}$  at 7.5 °K, and very satisfactory agreement was obtained with experiment.

### I. INTRODUCTION

Recently<sup>1</sup> one of us reported far-infrared absorption measurements on  $\text{LiF}$  at three temperatures and attempted to assign the features observed, together with higher-energy features reported elsewhere<sup>2</sup> in terms of specific two-phonon processes. The calculation was approximate inasmuch as the frequency-dependent frequency shift of the transverse-optic resonance was ignored and the intensity was scaled to fit experimental data. Thus it was also not possible to calculate the absorption due to the main resonance. The agreement in the far-infrared region where the absorption is due almost entirely to two-phonon "difference" processes was poor insofar as no features were predicted theoretically at all, whereas some structure was observed experimentally. Above the reststrahlen peak where two-phonon "summation" processes dominate, the calculated features differed considerably, both in magnitude and frequency from the reported experimental values. Most of the discrepancies in frequency were attributed to the "deformation-dipole" lattice-dynamical data, kindly supplied by Karo and Hardy, which differed in some regions from the frequencies measured by inelastic neutron diffraction.<sup>3</sup> Nevertheless it was possible to assign probable phonon-pairs to the experimental features.

This was accomplished first by consideration of certain criteria for strong coupling between specific phonon branches in different regions of the Brillouin zone, then by comparison of the calculated spectra with these predictions, and finally by referring to the frequencies measured by neutron scattering.

It was clear, however, that if shell-model lattice-dynamical data, which had been fitted to the inelastic-neutron dispersion curves, were used as input to the calculations, a great improvement would be obtained with respect to the shape and features of the spectrum. Building blocks of the shell-model program were kindly supplied by Dolling, and one of us (R. H.) has constructed a program which produces the data with a variable wave-vector density. Furthermore the calculations have now been performed on an absolute basis, starting with the values of frequency-dependent damping and frequency shift of the transverse optic resonance with near-zero wave vector ( $\vec{k} \sim 0$ ) and proceeding to the related optical constants of absorption coefficient, conductivity, dielectric constant, refractive index, reflectivity, etc. Thus by comparison of these quantities with various experimental results it was hoped to be able to answer some of the remaining questions in this area which may be summarized as follows. The agreement in frequency of features

will merely reflect the accuracy of the lattice-dynamical model and the ability of the model to generate accurate off-symmetry frequencies from fitting to those measured in major symmetry directions. The agreement in intensity, however, will depend on many things: the eigenvectors of the lattice model; the form and magnitude of the potential energy term used in the coupling coefficient calculation; the effect of the next-nearest neighbors on the coupling coefficient; the importance of higher-order phonon processes; the possible need to include the second-order electric moment along with anharmonicity; and the effect of impurities, especially natural isotopic impurities.

Information about some of these questions has been obtained from these calculations and is presented in the following sections, along with the theory and method of calculation. This method follows fairly closely the calculations which have been performed by Johnson and Bell<sup>4</sup> and Berg and Bell,<sup>5</sup> at room temperature only and with 1000 wave vectors per zone, for KCl and KI. They have not attempted to assign any particular phonon pairs to their spectral features.

## II. SHELL-MODEL CALCULATIONS

The basic theory of the shell model used in these calculations is described by Cochran *et al.*<sup>6</sup> Application of the model specifically to LiF is discussed by Dolling *et al.*,<sup>3</sup> and the choice of parameters used in this work correspond to their model I. For the purpose of comparison, notation for the parameters in the two references cited and the values used are given in Table I.

The physical assumptions of this particular model are that the short-range repulsive forces act entirely through the shells, that they are axially symmetric, and that they extend at most to second-nearest neighbors. The six *A* and *B* parameters specify this short-range force; *Z* is the ionic charge, and  $\alpha_i$  and  $d_i$  are, respectively, the electrical and mechanical polarizabilities of the *i*th ion. A computer program was written to use the University of British Columbia IBM/360 data pro-

TABLE I. Parameters used to specify the ionic interaction in LiF. The units are given in terms of the electronic charge *e* and the primitive cell volume *v*.

Parameter notation		Value	Unit
Ref. 6	Ref. 3		
A(12)	<i>A</i>	7.739	$e^2/2v$
B(12)	<i>B</i>	-0.874	$e^2/2v$
A(11)	<i>A'</i>	-0.317	$e^2/2v$
B(11)	<i>B'</i>	0.051	$e^2/2v$
A(22)	<i>A''</i>	1.030	$e^2/2v$
B(22)	<i>B''</i>	-0.056	$e^2/2v$
	<i>Z</i>	0.970	<i>e</i>
	$\alpha_1$	0.0062	1/ <i>v</i>
	$d_1$	-0.0270	<i>e</i>
	$\alpha_2$	0.0447	1/ <i>v</i>
	$d_2$	0.1460	<i>e</i>

cessing system to perform the following operations. For a given wave vector  $\vec{k}$ , the appropriate 6×6 dynamical matrix is set up to describe the collective motion of the two ionic species under their Coulomb interaction and the repulsive forces specified by the particular choice of parameters. Solution of the secular equation yields six eigenvalues (the acoustic- and optical-phonon frequencies), with their corresponding eigenvectors, which describe the polarization of the ionic motions. The procedure is repeated for a sequence of wave-vectors distributed uniformly throughout  $\frac{1}{48}$  of the volume of the Brillouin zone. The frequency eigenvalues obtained in each case have a multiplicity determined by the number of nonequal wave vectors generated by the operations of the cubic symmetry group. The complete set of corresponding eigenvectors is determined similarly by application of the appropriate symmetry operations.<sup>7</sup>

## III. THEORY AND CALCULATION OF THE TWO-PHONON PROCESSES

Wallis and Maradudin<sup>8</sup> and Cowley<sup>9</sup> have obtained an expression for the complex susceptibility of a cubic crystal with a first-order dipole moment, given by

$$\chi_\alpha(\bar{\nu}) = \chi_\infty + \frac{2}{Nv\hbar} \frac{\bar{\nu}(0, j_0) M_\alpha^2(0, j_0)}{\bar{\nu}^2(0, j_0) - \bar{\nu}^2 + 2\bar{\nu}(0, j_0) [\Delta(0, j_0; \bar{\nu}) - i\Gamma(0, j_0; \bar{\nu})]}, \quad (1)$$

where *N* is the number of unit cells in the crystal, *v* the volume of the unit cell, and  $\bar{\nu}(0, j_0)$  is the wave number (cm<sup>-1</sup>) of the degenerate transverse optic modes (*j*<sub>0</sub>) with wave vector  $\vec{k}$  effectively equal to zero. Equation (1) assumes a crystal with only two atoms per unit cell and therefore only one resonance.  $M_\alpha(0, j_0)$  is the  $\alpha$  coordinate of the dipole moment associated with the TO resonance, and

$\Delta(0, j_0; \bar{\nu})$  and  $\Gamma(0, j_0; \bar{\nu})$  are the frequency-dependent frequency shift and damping of the TO resonance.

If this damping of the TO resonance at wave number  $\bar{\nu}(0, j_0)$  is assumed to occur through relaxation to two phonons, and if the absorption at any wave number  $\bar{\nu}$  is assumed to be due to off-resonant excitation of the TO mode which then relaxes to two phonons with the same final combined wave number

$\bar{\nu}$ , then the damping may be written<sup>9</sup> in the form

$$\Gamma(0, j_0; \bar{\nu}) = \frac{18\pi}{\hbar^2}$$

$$\times \sum_{\vec{k}j_1} \sum_{-\vec{k}j_2} |V^{(3)}(0, j_0; \vec{k}, j_1; -\vec{k}, j_2)|^2 S(\bar{\nu}), \quad (2)$$

where  $V^{(3)}$  is the cubic coupling coefficient which couples the TO resonance to two other phonons which must have equal and opposite wave vectors  $\vec{k}$  (since the infrared photon momentum is so small), and in a crystal with center-of-inversion symmetry must belong to different polarization branches  $j_1$  and  $j_2$ .  $S(\bar{\nu})$  gives the temperature dependence through the phonon-occupation numbers, since both emission and absorption can occur, and also conserves energy in the process:

$$S(\bar{\nu}) = [n(\vec{k}, j_1) + n(-\vec{k}, j_2) + 1] \times \delta(\bar{\nu} - \bar{\nu}(\vec{k}, j_1) - \bar{\nu}(-\vec{k}, j_2)) \quad (3)$$

for the "summation" case in which two phonons are created and

$$S(\bar{\nu}) = [n(\vec{k}, j_1) - n(-\vec{k}, j_2)]$$

$$\times \delta(\bar{\nu} + \bar{\nu}(\vec{k}, j_1) - \bar{\nu}(-\vec{k}, j_2)) - \delta(\bar{\nu} - \bar{\nu}(\vec{k}, j_1) + \bar{\nu}(-\vec{k}, j_2)) \quad (4)$$

for the "difference" case in which one phonon is created and another is destroyed.

The Bose-Einstein occupation number  $n(\vec{k}, j)$  is given by

$$n(\vec{k}, j) = [e^{h\nu(\vec{k}, j)/ck_B T} - 1]^{-1}. \quad (5)$$

The coupling occurs through the third derivative  $\phi_{\alpha\beta\gamma}$  of the potential energy  $\phi$  between any two ions, and the full expression for  $V^{(3)}$ , which involves a triple product of displacements caused by the three phonons, was derived by Maradudin and is reproduced by Johnson and Bell.<sup>4</sup> Assuming the short-range repulsive component of  $\phi_{\alpha\beta\gamma}$  to predominate, so that only nearest-neighbor interactions need be considered, Johnson and Bell evaluated  $V^{(3)}$  for the rocksalt structure. The form given by Berg and Bell<sup>5</sup> is somewhat simplified and more correct. (This coupling coefficient has also been evaluated for the CsCl structure.<sup>10</sup>)

Using those results, the damping term in  $\text{cm}^{-1}$ , abbreviated to  $\Gamma(\bar{\nu})$  may be written

$$\Gamma(\bar{\nu}) = \frac{\pi\hbar(M^+ + M^-)}{4N(2\pi c)^5(M^+ M^-)^2 \bar{\nu}(0, j_0)} \sum_{\vec{k}j_1} \sum_{-\vec{k}j_2} [\bar{\nu}(\vec{k}j_1) \bar{\nu}(-\vec{k}j_2)]^{-1} S(\bar{\nu}) \left\{ \left[ \phi'''(r_0) [m_x^+(\vec{k}j_1) m_x^-(\vec{k}j_2) - m_x^-(\vec{k}j_1) m_x^+(\vec{k}j_2)] + \left( \frac{\phi''(r_0)}{r_0} - \frac{\phi'(r_0)}{r_0^2} \right) \sum_{\alpha=y,z} [m_\alpha^+(\vec{k}j_1) m_\alpha^-(\vec{k}j_2) - m_\alpha^-(\vec{k}j_1) m_\alpha^+(\vec{k}j_2)] \right] \times \sin(2\pi r_0 k_x) + \left( \frac{\phi''(r_0)}{r_0} - \frac{\phi'(r_0)}{r_0^2} \right) \sum_{\alpha=y,z} \{ [m_\alpha^+(\vec{k}, j_1) m_\alpha^-(\vec{k}, j_2) - m_\alpha^-(\vec{k}, j_1) m_\alpha^+(\vec{k}, j_2)] \sin(2\pi r_0 k_\alpha) \}^2 \right\}, \quad (6)$$

where  $M^+$ ,  $M^-$  are the masses of the  $\text{Li}^+$  ion and  $\text{F}^-$  ion,  $\phi'''(r_0)$  and  $\phi''(r_0)$  are the third and second radial derivatives of the potential energy at an ion site due to a nearest neighbor, evaluated at equilibrium,  $r_0$  is the nearest-neighbor separation, and  $m_\alpha^+(\vec{k}, j)$  is the  $\alpha$  component of the normalized  $\text{Li}^+$  eigenvector associated with the mode  $\vec{k}, j$ .

There are various forms of expression<sup>4,5</sup> for the frequency shift  $\Delta(0, j_0; \bar{\nu})$ , but for the purpose of the calculations performed here, it was found convenient to express it through the Kramers-Kronig relationship, which relates the real and imaginary parts of the complex frequency shift. Thus abbreviating to  $\Delta(\bar{\nu})$ ,

$$\Delta(\bar{\nu}) = + \frac{2}{\pi} \int_0^{\bar{\nu}_M} \frac{\bar{\nu}'}{\bar{\nu}^2 - \bar{\nu}'^2 + \epsilon^2} \Gamma(\bar{\nu}') d\bar{\nu}' + \text{const} \quad (7)$$

was the form used, with  $\bar{\nu}_M$  taken just beyond the two-phonon limit and  $\epsilon$  set to a small number. The frequency-dependent shifts caused for example by

thermal expansion have not been calculated since their effect is compensated by use of the experimental values of  $\bar{\nu}_0$  (see Sec. IIIB).

#### A. Potential Energy

Assuming that the equilibrium potential energy at a  $\text{LiF}$  ion site, due to the attractive Coulomb interaction of the entire lattice and the short-range repulsive interaction of the nearest neighbors only, is of the form

$$\phi(r_0) = - \frac{\alpha' e^2}{r_0} + 6C e^{-r_0/\rho}, \quad (8)$$

where  $\alpha'$  is the Madelung constant (equal to 1.7476 when  $r_0$  is the nearest-neighbor separation) and  $e$  is the electronic charge, then  $C$  and  $\rho$ , the repulsive parameters, may be obtained from temperature-dependent experimental values of compressibility,  $\beta$  and  $r_0$ , as follows:

$$\rho = \frac{r_0 \beta \alpha' e^2}{2\beta \alpha' e^2 + 18 r_0^4} \quad (9)$$

and

$$C = \frac{\alpha' e^2 \rho e^{r_0/\rho}}{6r_0^2} \quad (10)$$

In the evaluation of  $V^{(3)}$ , however, the functions  $\phi'''(r_0)$ ,  $\phi''(r_0)$ , and  $\phi'(r_0)$  were the third, second, and first radial derivatives of the potential energy due to a pair of nearest neighbors (NN) only, in equilibrium. Considering the third derivative, then,

$$\phi'''_{NN}(r_0) = \frac{6e^2}{r_0^4} - \frac{C e^{-r_0/\rho}}{\rho^3} \quad (11)$$

It is not sufficient to ignore the Coulombic first term since with the values of  $C$  and  $\rho$  obtained from Eqs. (9) and (10), (using room-temperature values of  $r_0$  and  $\beta$ ; see Table II), the first and second terms in Eq. (11) equal  $8.49 \times 10^{12}$  and  $-18.65 \times 10^{12}$  erg cm<sup>-3</sup>. It should also be noted that  $\phi'''(r_0)$  is squared in the final form for  $\Gamma(\bar{\nu})$ . To leave  $\phi'''(r_0)$  as it stands, however, will produce too low a value of  $\Gamma(\bar{\nu})$  since no account of the coupling produced by the motion of other-than-nearest neighbors has been considered. Although the repulsive component of  $\phi'''_{NN}(r)$  will rapidly decrease, the Coulombic component,  $6e^2/r^4$ , will oscillate in sign and decrease slowly since neighbors increase as  $r^3$ . To account for next-nearest neighbors (NNN) exactly would be difficult, not only because of the tedious calculation of the coupling coefficient, but also because the values of  $C_{NNN}$  and  $\rho_{NNN}$  are not known since the ions are alike rather than opposite as in Eq. (11). Even if an estimate were made for  $C_{NNN}$  and  $\rho_{NNN}$ , one would have to return to Eq. (8) and include the NNN contribution before  $C$  and  $\rho$

could be determined. Also of course, other than next-nearest neighbors would still be neglected. A compromise was therefore reached. It was decided to let the coupling coefficient due to all neighbors be of the same form as that for the nearest neighbors. This will overaccentuate the features produced in the calculated spectrum. It is far preferable, however, to completely unrestricted coupling since it has been seen<sup>1</sup> that this allows far too great a coupling between low-energy acoustic phonons. A correction may now be made to Eq. (11). Leaving the repulsive component as it stands [since in effect all neighbors have been included in Eq. (8)], the total Coulombic term at one lattice site due to the entire lattice may be written

$$\phi'''_T(\text{Coulombic}) = \frac{6\alpha'' e^2}{r_0^4} \quad (12)$$

or normalized to one NN pair

$$\phi'''_{N.T.}(\text{Coulombic}) = \frac{\alpha'' e^2}{r_0^4} \quad (13)$$

where  $\alpha''$  is a constant defined by

$$\alpha'' = \frac{1}{2e^2} \sum_k \sum_{l \neq k} \frac{r_0^4 e_k e'_k}{|x(k) - x(l)|^4} \quad (14)$$

Such a sum will oscillate in sign and must be evaluated separately for each sign if the simple procedure outlined in Born and Huang<sup>11</sup> may be followed:

$$\sum_l' \frac{1}{|x(l)|^n} = \sum_{|x(l)| < R} \frac{1}{|x(l)|^n} + \frac{1}{(3N)^{(1/3)n-1} (v-3)} \left( \frac{4\pi}{v} \right)^{n/3} \quad (15)$$

where  $v$  is the cell volume. This sum was per-

TABLE II. Some constants used in the calculations.

		300 °K	0 °K
Resonant absorption wave number <sup>a</sup>	$\bar{\nu}_0$	305 cm <sup>-1</sup>	318 cm <sup>-1</sup>
Static dielectric constant <sup>a</sup>	$\epsilon_0$	9.0	8.5
High-frequency dielectric constant <sup>a</sup>	$\epsilon_\infty$	1.926	1.933
Lattice constant <sup>b</sup>	$r_0$ (10 <sup>-8</sup> cm)	2.0087	2.0004
Compressibility <sup>b</sup>	$\beta$ (10 <sup>-12</sup> /bar)	1.54	1.43
Repulsive overlap potential parameters	$C$ (10 <sup>-10</sup> erg)	4.148	5.278
	$\rho$ (10 <sup>-3</sup> cm)	0.2986	0.2856
Third potential derivative	$\phi'''_{N.T.}(r_0)$ (10 <sup>12</sup> erg cm <sup>-3</sup> )	-13.19	-15.01
Second potential derivative	$\phi''_{N.T.}(r_0)/r_0$ (10 <sup>12</sup> erg cm <sup>-3</sup> )	0.95	1.09
First potential derivative	$\phi'_{N.T.}(r_0)/r_0^2$ (10 <sup>12</sup> erg cm <sup>-3</sup> )	0.50	0.51
Szigeti effective charge	$e^*/e$	0.80	0.81

<sup>a</sup>See Ref. 13.

<sup>b</sup>See Ref. 14.

formed on like ions and unlike ions taking  $R$  to include 50 "shells" of nearest neighbors. The difference between the two converged fairly rapidly to give

$$\alpha'' = 3.862 \pm 0.002. \quad (16)$$

Thus the final form for  $\phi''''(r_0)$  became

$$\phi''''_{N.T.}(r_0) = \frac{\alpha'' e^2}{r_0^4} - \frac{C e^{-r_0/\rho}}{\rho^3}. \quad (17)$$

Likewise the final forms for  $\phi''(r_0)/r_0$  and  $\phi'(r_0)/r_0^2$  were taken as

$$\frac{\phi''_{N.T.}(r_0)}{r_0} = -\frac{\alpha'' e^2}{3r_0^4} + \frac{C e^{-r_0/\rho}}{r_0 \rho^2} \quad (18)$$

and

$$\frac{\phi'_{N.T.}(r_0)}{r_0^2} = \frac{\alpha'' e^2}{6 r_0^4} - \frac{C e^{-r_0/\rho}}{r_0^2 \rho}. \quad (19)$$

The room-temperature and zero-degree values used may be found in Table II. Intermediate-temperature values were obtained by interpolation.

#### B. $\Gamma(0, j_0; \bar{\nu})$ and $\Delta(0, j_0; \bar{\nu})$

A program was written which calculated  $\Gamma(\bar{\nu})$  (abbreviated) for the difference and summation processes separately, although of course the bulk of the calculation was common to both. The input lattice-dynamical data were on tape and consisted of eigendata for a uniform wave-vector grid in the irreducible  $\frac{1}{48}$ th of the Brillouin zone as described in Sec. II. It was found unnecessary to apply the point-group symmetry operators to the eigendata associated with one wave vector in order to generate all the symmetry-related data throughout the zone. This was due to the high symmetry of  $\Gamma(\bar{\nu})$

as written in Eq. (6) such that  $\Gamma(\bar{\nu})$  was invariant with respect to reflection of the wave-vector coordinates and interchange of  $y$  and  $z$ , but changed only with rotation. Thus three  $\Gamma(\bar{\nu})$ 's were calculated for each  $\bar{k}, j_1; -\bar{k}, j_2$ , one as written in Eq. (6) and the other two with  $y$  and  $z$  replacing  $x$ , respectively. The multiplicity was then calculated and used to give the correct density of states. Another factor of 2 in time could be saved by summing over  $j_1$  and  $j_2 > j_1$  and doubling the result. Since the program was so rapid, it was found possible to use generated lattice-dynamical data with a wave-vector density of 256 000 points per zone, corresponding to 6281 points in the irreducible zone volume. It is this latter figure that determines the resolution possible in  $\Gamma(\bar{\nu})$  and  $\Delta(\bar{\nu})$ . The values of  $\Gamma(\bar{\nu})$  were assigned to the nearest integral wave number and the result smoothed by convoluting with a 17-point least-squares fit to a cubic polynomial<sup>12</sup> (quadratic in wave number). This smoothing does not broaden or reduce the peak heights of real features with a resolution of  $5 \text{ cm}^{-1}$  or so (a compromise between the best and worst parts of the spectrum) but does eliminate a great deal of noise. The calculation of  $\Gamma(\bar{\nu})_{\text{DIFF}}$  and  $\Gamma(\bar{\nu})_{\text{SUM}}$  for one temperature took under 3 min on an IBM 360/67.

$\Delta(\bar{\nu})$  was calculated from Eq. (7) putting  $\epsilon$  extremely small ( $10^{-3} \text{ cm}^{-1}$ ) so that the resolution of  $\Delta(\bar{\nu})$  was the same as that for  $\Gamma(\bar{\nu})_{\text{TOTAL}}$ . The computer took around two minutes with  $\bar{\nu}_M$  set equal to  $1200 \text{ cm}^{-1}$  and  $d\bar{\nu}'$  equal to  $1 \text{ cm}^{-1}$ . The unknown constant is immaterial since  $\Delta(0, j_0; \bar{\nu}_0)$  is subtracted from  $\Delta(0, j_0; \bar{\nu})$  in order that the frequency shift is zero at the measured resonant frequency  $\bar{\nu}_0$ . Thus Eq. (1) becomes

$$\chi_\alpha(\bar{\nu}) = \chi_\infty + \frac{2}{Nv\hbar} \frac{\bar{\nu}_0 M_\alpha^2(0, j_0)}{\bar{\nu}_0^2 - \bar{\nu}^2 + 2\bar{\nu}_0 [\Delta(0, j_0; \bar{\nu}) - \Delta(0, j_0; \bar{\nu}_0) - i\Gamma(0, j_0; \bar{\nu})]}. \quad (20)$$

Figures 1 and 2 show the calculated  $\Gamma(\bar{\nu})$ 's, difference and summation, at 300 and 77 °K. Note the scale for  $\Gamma(\bar{\nu})_{\text{DIFF}}$  at 77 °K. The curves have not been hand-smoothed at all, so that in regions of low combined density of states, a sampling "ripple" due to the steep frequency-dispersion curve of at least one of the contributing phonons may be seen [e.g., between 400 and 650  $\text{cm}^{-1}$  for  $\Gamma(\bar{\nu})_{\text{DIFF}}$ ]. This occurs despite the high wave-vector density of 256 000 per zone but is reduced by the smoothing.

Two points are worthy of attention here, apart from the assignments of the structure, which will be dealt with shortly. First it may be seen that  $\Gamma(\bar{\nu})_{\text{SUM}}$  is zero at  $\bar{\nu}_0$  so that the height of the main resonance will be determined merely by the differ-

ence processes, as far as two-phonon relaxation is concerned. The fact that  $\Gamma(\bar{\nu})_{\text{SUM}}$  is zero at low energies is a result of the low coupling between any two low-energy acoustic modes, since the relative displacement of nearest-neighbor ions due to the superposition of long-wavelength acoustic waves is so small. Second,  $\Gamma(\bar{\nu})_{\text{DIFF}}$  itself is small at  $\bar{\nu}_0$  (almost a minimum at 77 °K, purely coincidental of course) so that it should be fairly easy to detect the higher-phonon relaxation, as the temperature is raised, from the resonance peak height and width.

Figure 3 shows  $\Delta(\bar{\nu}) - \Delta(\bar{\nu}_0)$ , once again for 300 and 77 °K.

#### C. Two-Phonon Assignments

The criteria for strong coupling of the TO mode to two other phonons in the rocksalt lat-

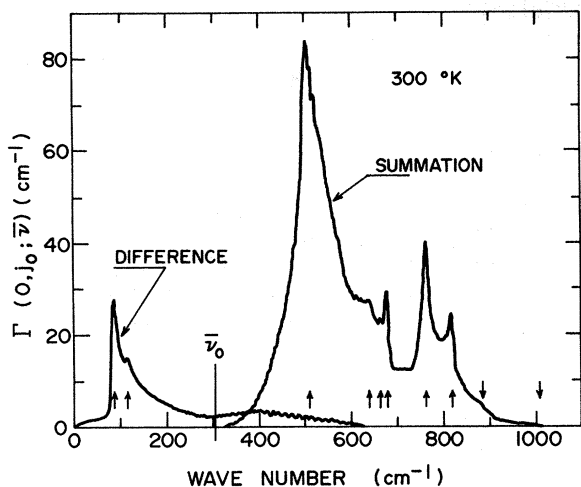


FIG. 1. The calculated 300 °K damping of the transverse-optic mode at zero wave vector via two-phonon summation and two-phonon difference processes,  $\Gamma(0, j_0; \bar{\nu})$ .

tice have already been reported.<sup>1</sup> Briefly they comprise (1) frequency-dispersion-curve slope matching (equal and opposite for summation, equal and parallel for difference), (2) an eigenvector requirement of each combining phonon having at least one eigenvector Cartesian component in the same direction, and (3) positioning in the Brillouin zone to maximize a sine-term modulation, which with nearest-neighbor interaction gives, for example, zero coupling at X. The nearest-neighbor approximation also gives zero coupling when one ion is at rest in both modes. Finally it should be repeated that at low temperature the intensity of the "difference" absorption processes depends strongly on the energy of the destroyed pho-

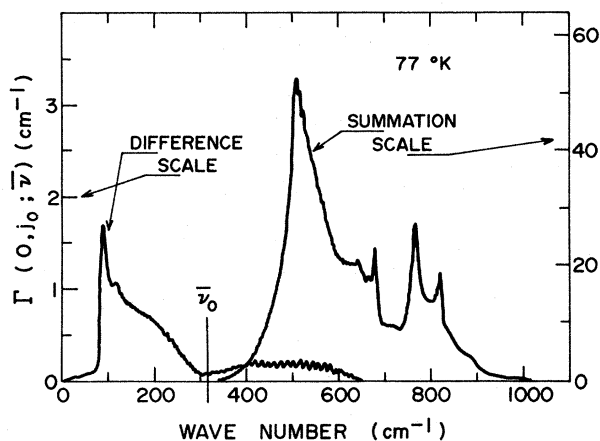


FIG. 2. The calculated 77 °K damping of the transverse-optic mode at zero wave vector via two-phonon summation and two-phonon difference processes,  $\Gamma(0, j_0; \bar{\nu})$ .

non.

Arrows have been included in Fig. 1 to show the positions of the features in the calculated  $\Gamma(\bar{\nu})$  spectrum at 300 °K. These will be responsible for any structure observed experimentally in any of the optical constants, but their relative magnitude may be altered (see Sec. III D). Table III lists the arrowed features and the major contributing phonon pairs at that wave number. Most of the combinations expected on the basis of the above criteria<sup>1</sup> are found to be responsible for some feature or other, although some merge together to form rather broad maxima. As mentioned elsewhere, apart from the four strong combinations at the high-symmetry point  $L$ , the remaining combinations come from less-well-defined regions along  $\Sigma$ , and near  $Q$ ,  $W$ ,  $U$ , and  $Z$ . Sometimes a minor contributor in one of these regions may be responsible for a weak maximum on top of a large background, and thus is difficult to assign.

The high-symmetry dispersion curves (298 °K) are given by Dolling.<sup>3</sup> Some less symmetrical directions are shown in Fig. 4, where the branches from  $\Gamma$  to  $W$  and  $Q$  have been arbitrarily labeled.

A few comments are in order on the predictions in Ref. 1. The 87-cm<sup>-1</sup> peak does not seem to resolve the  $L'_3L_3$  and  $\Sigma_4\Sigma_4$  pairs. The  $\Delta_5\Delta_5$  contribution at 115 cm<sup>-1</sup> is probably not as great as that from the region around  $Q$ . No  $\Sigma_4\Sigma_4$  maximum is evident by itself around 488 cm<sup>-1</sup>, but combines with the strong  $L'_3L_3$  and fortuitous  $\Gamma \rightarrow Q$  to give the large 510-cm<sup>-1</sup> peak.  $W'_2 + W_1$  does not seem to combine strongly since their surrounding slopes are equal and not opposite and also there appears no maximum due to  $\Delta_1\Delta_1$ .

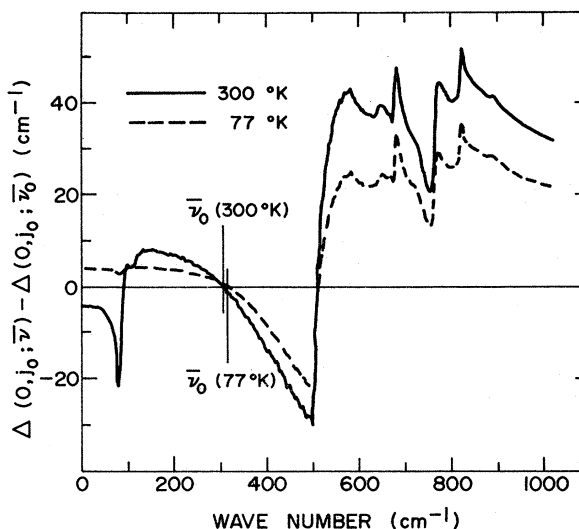


FIG. 3. The calculated 300 and 77 °K frequency shift of the transverse-optic mode at zero wave vector via two-phonon summation and difference processes,  $\Delta'(0, j_0; \bar{\nu})$ .

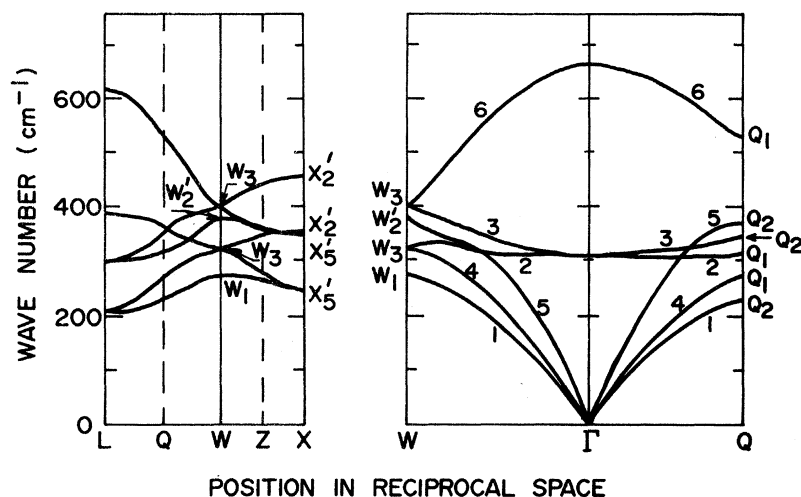


FIG. 4. The frequency-dispersion curves produced by the shell model I, fitted to the neutron measurements of Dolling *et al.* (Ref. 3) on LiF at 298 °K, in some less-symmetrical directions.

#### D. Optical Properties

The various experimental investigations of LiF in the past have either been transmission measurements, giving absorption coefficients directly or reflection measurements which may be analyzed either by a Kramers-Kronig analysis or a classical-oscillator model to give real and imaginary optical constants. All of these constants have therefore been calculated and compared with whatever experimental data are available.

##### 1. Real Dielectric Constant $\epsilon'$

The real dielectric constant  $\epsilon'$  is given by

$$\epsilon' = \epsilon_{\infty} + 4\pi \text{Re}(\chi). \quad (21)$$

From Eq. (20) and expressing  $M_{\alpha}(0, j_0)$  as in Ref. 4, this becomes

$$\epsilon'(\bar{\nu}) = \epsilon_{\infty} + \frac{e_i^{*2}(M^+ + M^-)[\bar{\nu}_0^2 - \bar{\nu}^2 + 2\bar{\nu} \Delta'(\bar{\nu})]}{\pi \nu c^2 M^+ M^- \{[\bar{\nu}_0^2 - \bar{\nu}^2 + 2\bar{\nu}_0 \Delta'(\bar{\nu})]^2 + 4\bar{\nu}_0^2 \Gamma^2(\bar{\nu})\}}, \quad (22)$$

where

$$\Delta'(\bar{\nu}) = \Delta(0, j_0; \bar{\nu}) - \Delta(0, j_0; \bar{\nu}_0) \quad (23)$$

and

$$e_i^* = \frac{1}{3} e^*(\epsilon_{\infty} + 2) \quad (24)$$

with  $e^*$  the Szigeti effective charge.

From Eq. (22) it is clear that

TABLE III. The two-phonon assignments of the calculated  $\Gamma(0, j_0; \bar{\nu})$  spectrum at 300 °K (underlined numbers refer to Fig. 4 labels).

Wave Number (cm <sup>-1</sup> )	Strength		Process	Major contributing phonon pairs, with strength			
	S-Strong	M-Medium		S-Strong	M-Medium	W-Weak	V-Very
87	S		Diff	$L_3' - L_3$ (S), $\Sigma_4 - \Sigma_4$ (S), $Q$ ( <u>2-1</u> ) (S)			
115	W		Diff	$\Lambda_3 - \Lambda_3$ (S), $\Sigma_4 - \Sigma_4$ (W), $Q$ ( <u>3-1</u> ) (M), $\Delta_5 - \Delta_5$ (W)			
510	VS		Sum	$L_3' + L_3$ (VS), $\Gamma \rightarrow Q$ ( <u>1+2</u> ) (M)			
640	W		Sum	$\Sigma_1$ (LA) + $\Sigma_4$ (TO) (W), $\Gamma \rightarrow W$ ( <u>2+5</u> ) (W)			
665	W		Sum	$\Gamma \rightarrow Q$ ( <u>2+3</u> ), $\Gamma \rightarrow U$ , $\Gamma \rightarrow W$ (All W)			
680	M		Sum	$L_3' + L_1$ (S), $Q$ ( <u>2+5</u> ) (S)			
765	S		Sum	$\Sigma_1$ (LO) + $\Sigma_4$ (TA) (S)			
820	M		Sum	$L_3 + L_1'$ (M), $\Sigma_1$ (LO) + $\Sigma_4$ (TO) (M)			
885	VW		Sum	$\Sigma_1 + \Sigma_1$ (W)			
1010	2-phonon limit			$L_1 + L_1'$			

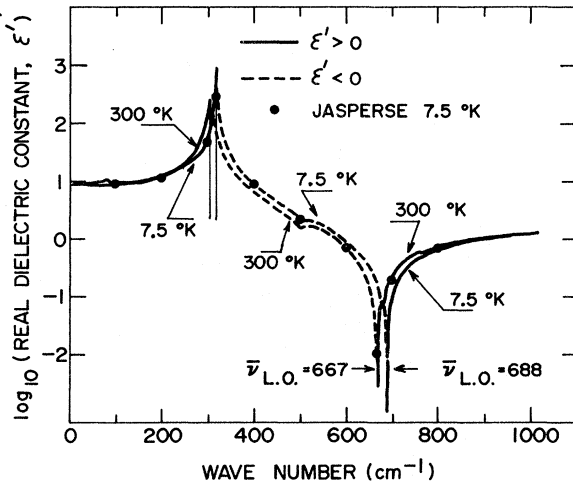


FIG. 5. The calculated real dielectric constant  $\epsilon'$  at 300 and 7.5 °K, using two-phonon relaxation only (i. e., Li<sup>7</sup>F) with some points taken from the reflectivity analysis of natural LiF of Jasperse *et al.* (Ref. 15) at 7.5 °K.

$$\epsilon_0 = \epsilon_\infty + \frac{e_i^{*2}(M^+ + M^-)}{\pi \nu c^2 M^+ M^- \bar{\nu}_0^2 [1 + 2\Delta'(0)/\bar{\nu}_0]} \quad (25)$$

Equation (25) differs from the harmonic approximation only by the extra "static" frequency-shift term in the denominator. The harmonic form of Eq. (25) was used by Lowndes and Martin<sup>13</sup> to calculate  $e^*$ , using their measured values of  $\epsilon_\infty$ ,  $\epsilon_0$ , and  $\bar{\nu}_0$ . They obtained 0.81 (290 °K) and 0.80 (2 °K) for  $e^*$ . Using once again their measured input values, which may be found in Table II, together with our calculated values of  $\Delta'(0)$  [ $-4 \text{ cm}^{-1}$  (300 °K) and  $+4 \text{ cm}^{-1}$  (0 °K)] the values for the Szegedi effective charge, with corrections for anharmonicity, were calculated to be 0.80 (300 °K) and 0.81 (0 °K). These were then used in the calculation of  $\epsilon'(\bar{\nu})$ .

The 300 and 7.5 °K values of  $\epsilon'$  may be seen in Fig. 5 together with some 7.5 °K points from Jasperse *et al.*<sup>15</sup> Jasperse *et al.* performed a two-resonance damped-oscillator model analysis of the reflectivity of natural LiF, a procedure with little physical basis but capable of yielding optical constants which reproduced the measured reflectivity satisfactorily. This is because of the large peak in  $\Gamma(\bar{\nu})$  around 500  $\text{cm}^{-1}$ . Nevertheless the data of Jasperse *et al.* will be reliable only between  $\bar{\nu}_0$  and the frequency of the zero-wave-vector longitudinal-optic mode,  $\bar{\nu}_{\text{LO}}$ , in which region the reflectivity is high. Between 200  $\text{cm}^{-1}$  and  $\bar{\nu}_0$  the imaginary optical constants will be unreliable since they are so small in comparison with the real constants, and none of the subsidiary structure beyond  $\bar{\nu}_{\text{LO}}$  will be predicted. The calculated constants of Jasperse *et al.* are essentially in agreement with those calculated from a Kramers-Kronig analysis

by Frohlich.<sup>16,17</sup> (The analysis by Gottlieb<sup>18</sup> differs somewhat and does not even show a temperature dependence of  $\bar{\nu}_0$ ).

The agreement in Fig. 5 is satisfactory except for the predicted LO frequencies,  $\bar{\nu}_{\text{LO}}$ , obtained when  $\epsilon'$  goes through zero. The Lyddane-Sachs-Teller relation, which is quickly obtained from the harmonic form of Eq. (22), gives

$$\bar{\nu}_{\text{LO}}^2 / \bar{\nu}_0^2 = \epsilon_0 / \epsilon_\infty \quad (26)$$

Using the values in Table II, Eq. (26) predicts  $\bar{\nu}_{\text{LO}}$  to be 659  $\text{cm}^{-1}$  at 300 °K and 667  $\text{cm}^{-1}$  at 0 °K.

With the inclusion of cubic anharmonicity, however, a more accurate relation than Eq. (26) may be readily obtained, from Eq. (22),

$$\frac{\bar{\nu}_{\text{LO}}^2}{\bar{\nu}_0^2} = \frac{\epsilon_0}{\epsilon_\infty} \left( 1 + \frac{2\Delta'(0)}{\bar{\nu}_0} \right) + \frac{2}{\bar{\nu}_0} [\Delta'(\bar{\nu}_{\text{LO}}) - \Delta'(0)] \quad (27)$$

This relation predicts  $\bar{\nu}_{\text{LO}}$  wave-number values of 667  $\text{cm}^{-1}$  at 300 °K and 688  $\text{cm}^{-1}$  at 7.5 °K, as shown in Fig. 5. [The calculated values of  $\Delta'(\bar{\nu}_{\text{LO}})$  are  $+38 \text{ cm}^{-1}$  (300 °K) and  $+28 \text{ cm}^{-1}$  (7.5 °K).]

The room-temperature wave number  $\bar{\nu}_{\text{LO}}$  for Li<sup>7</sup>F measured by neutron diffraction is 657  $\text{cm}^{-1}$ , which may be scaled to 661  $\text{cm}^{-1}$  for natural LiF. This unfortunately is closer to the harmonic prediction than the anharmonic one, casting some doubt on the calculated frequency shifts. [The measured value quoted by Jasperse *et al.* for natural LiF is 672  $\text{cm}^{-1}$ , and by Berreman (see Ref. 15) is 670  $\text{cm}^{-1}$ , but these are probably not as reliable as the neutron value.]

The 7.5 °K value of Jasperse *et al.* is about 670  $\text{cm}^{-1}$ , as shown in Fig. 5, also closer to the harmonic prediction, but no value measured by neutrons exists.

The faint structure in  $\epsilon'$  at 90, 500, 680, 760, and 820  $\text{cm}^{-1}$  is due to  $\Delta'(\bar{\nu})$  in the denominator of Eq. (22) since the effect of  $\Gamma(\bar{\nu})$  is negligible away from  $\bar{\nu}_0$ .

## 2. Imaginary Dielectric Constant $\epsilon''$

The imaginary dielectric constant  $\epsilon''$  is given by

$$\epsilon'' = 4\pi \text{Im}(\chi) \quad (28)$$

Figure 6 shows the 300 and 7.5 °K calculated data, using Eqs. (20) and (28), with that of Jasperse *et al.* As expected, the data of Jasperse *et al.* include no structure below  $\bar{\nu}_0$  or above  $\bar{\nu}_{\text{LO}}$  but there is agreement with the maximum around 500  $\text{cm}^{-1}$ . The calculated resonance, however, appears to be too high and sharp at 300 °K with the discrepancy becoming extreme at 7.5 °K.

## 3. Extinction Coefficient $k$

Using the notation,  $\hat{n} = n + ik$ ,  $\hat{\epsilon} = \epsilon' + i\epsilon''$ , and  $\hat{n} = \hat{\epsilon}^{1/2}$ ,  $k$  may be found from  $\epsilon'$  and  $\epsilon''$ ,

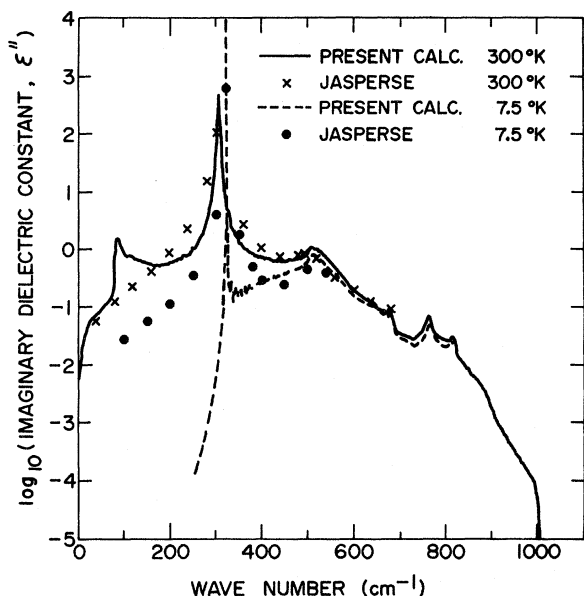


FIG. 6. The calculated imaginary dielectric constant  $\epsilon''$  at 300 and 7.5 °K for  $\text{Li}^7\text{F}$  with some points from Jasperse *et al.* for natural  $\text{LiF}$ .

$$k^2 = \frac{1}{2}(|\hat{\epsilon}| - \epsilon'). \quad (29)$$

The 300 °K calculated spectrum is shown in Fig. 7 together with the experimental results of Frohlich<sup>17</sup> and an average of those obtained directly from transmission measurements by Hohls<sup>19</sup> and Klier<sup>20</sup> (see Mitskevich<sup>21</sup>). The agreement is good, including the 500- $\text{cm}^{-1}$  change of slope, until the obvious need for multiphonon contributions above 800  $\text{cm}^{-1}$ . It may be noted that between  $\bar{\nu}_0$  and  $\bar{\nu}_{\text{LO}}$ , where  $\epsilon'$  is negative, the structure comes mainly

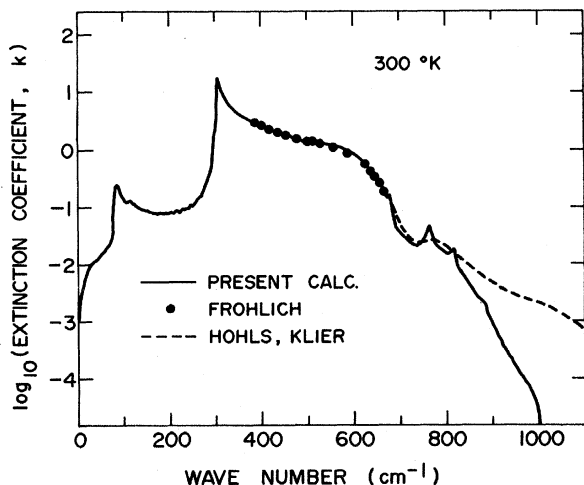


FIG. 7. The calculated extinction coefficient  $k$  at 300 °K for  $\text{Li}^7\text{F}$ , with the data of Frohlich (Ref. 17) and an average of the data of Hohls (Ref. 19) and Klier (Ref. 20).

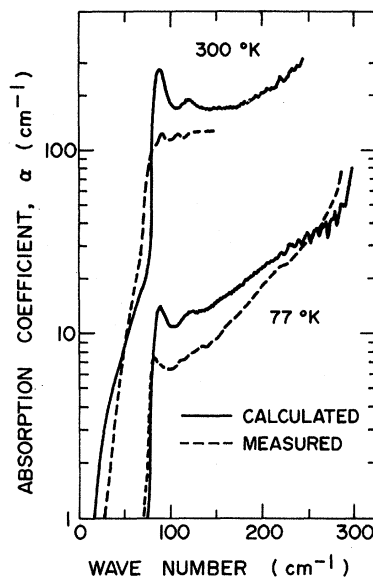


FIG. 8. The calculated absorption coefficient  $\alpha$  at 300 and 77 °K for  $\text{Li}^7\text{F}$ , with the measured data of Eldridge (Ref. 1) on natural  $\text{LiF}$ , below  $\bar{\nu}_0$ .

from  $\epsilon'$  [i. e., from the small effect of  $\Delta'(\bar{\nu})$  in the denominator], whereas outside this range, the structure is almost linearly proportional to  $\Gamma(\bar{\nu})$ .

#### 4. Absorption Coefficient $\alpha$

The absorption coefficient  $\alpha$  is obtained directly from  $k$ , since  $\alpha = 4\pi k\bar{\nu}$ . Figure 8 shows the low-energy results for two temperatures together with the measurements already reported by one of us.<sup>1</sup> (The 55 °K data have been omitted for clarity.) The agreement is good insofar as the features around 90 and 120  $\text{cm}^{-1}$  are concerned, and a vast improvement on that previously obtained using the deformation-dipole data.<sup>1</sup> There remains, however, the intensity discrepancy. Figure 9 shows  $\alpha$  over the entire range, this time at 7.5 and 300 °K in comparison with the results of Jasperse *et al.* at 7.5 °K, the low-energy absorption measurements in  $\text{Li}^7\text{F}$  of Eldridge<sup>22</sup> at 10 °K, and the 300 °K measurements shown in Fig. 8. The agreement with the Eldridge measurements and the Jasperse data between  $\bar{\nu}_0$  and  $\bar{\nu}_{\text{LO}}$  is good. It is apparent, however, that the present calculations which have not included the isotope-induced one-phonon absorption<sup>22</sup> [natural  $\text{LiF}$  is  $\text{Li}^7$ (92.5 at.%)  $\text{Li}^6$ (7.5 at.%)F] and therefore apply only to  $\text{Li}^7\text{F}$  should not be expected to agree with the low-temperature data of Jasperse *et al.* at and below  $\bar{\nu}_0$ .

#### 5. Refractive Index $n$

The refractive index  $n$  was calculated from  $\epsilon''$  and  $k$ , since  $\epsilon'' = 2nk$ , and may be seen for 300 and 7.5 °K in Fig. 10. Obviously between  $\bar{\nu}_0$  and  $\bar{\nu}_{\text{LO}}$ ,

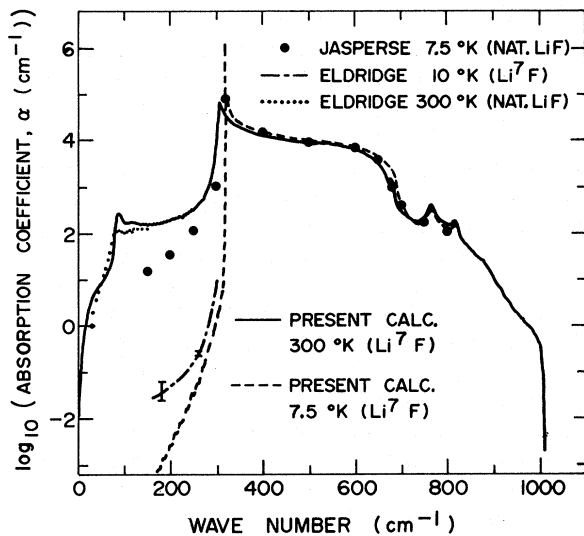


FIG. 9. The calculated absorption coefficient  $\alpha$  at 300 and 7.5 °K for  $\text{Li}^7\text{F}$  over the entire spectrum, with the natural LiF data of Jasperse *et al.* (Ref. 15) and Eldridge (Ref. 1) and the 10 °K  $\text{Li}^7\text{F}$  data of Eldridge (Ref. 22).

$n$  will contain the structure in  $\epsilon''$  [proportional to  $\Gamma(\nu)$ ] which was lost in  $k$ , and outside this region will be fairly smooth. Once again the low-temperature comparison at  $\bar{\nu}_0$  is invalid, but the calculated 300 °K resonance is also too sharp. At 500  $\text{cm}^{-1}$  the calculated peak appears too high. Elsewhere the agreement is good.

#### 6. Reflectivity $R$ and Phase Angle $\theta$

The power reflectivity  $R$  and phase angle  $\theta$  were obtained from the relations

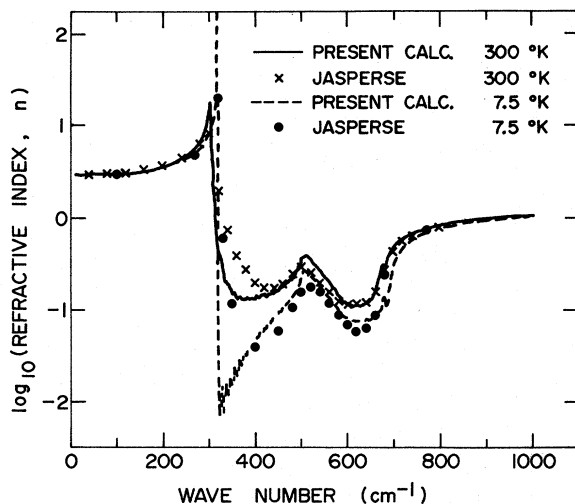


FIG. 10. The calculated refractive index  $n$  at 300 and 7.5 °K for  $\text{Li}^7\text{F}$ , with some points from the natural LiF data of Jasperse *et al.*

$$R = |\hat{r}|^2, \quad (30)$$

where

$$\hat{r} = re^{i\theta} = \frac{n+ik-1}{n+ik+1} \quad (31)$$

for normal reflectance.

The results in Fig. 11 show that the calculated values are too high between 300 and 400  $\text{cm}^{-1}$  and too low at 500  $\text{cm}^{-1}$ . The latter is due to the calculated  $n$  being too high at 500  $\text{cm}^{-1}$ . The 7.5 °K comparison is once again strictly invalid at  $\bar{\nu}_0$ . Elsewhere the agreement is good. The phase angle is included for interest, showing that any high-energy structure would be extremely difficult to detect from  $R$  and would require either a direct absorption measurement or a reflectance phase and amplitude measurement by asymmetric Fourier spectroscopy as in Refs. 4 and 5.

#### E. Discussion

Apart from the predicted LO frequencies, three discrepancies are obvious from the results in Sec. III D. First one must include the effects of the  $\text{Li}^6$  isotopic impurity if low-temperature comparisons are to be made with the results from natural LiF. (Apart from Ref. 22 no other low-temperature work on  $\text{Li}^7\text{F}$  is known.) This should affect only the region around the  $\bar{\nu}_0$  resonance, and below, where  $\Gamma(\bar{\nu})$  due to the difference processes is negligible by 7.5 °K, and because the strong sum-

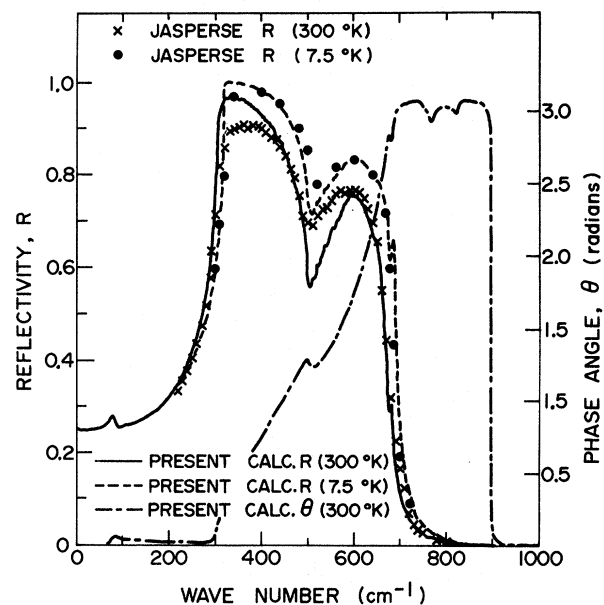


FIG. 11. The calculated reflectivity  $R$  at 300 and 7.5 °K for  $\text{Li}^7\text{F}$ , with the calculated phase angle  $\theta$  at 300 °K for  $\text{Li}^7\text{F}$ , and all of the 300 °K (some of the 7.5 °K) measured values of reflectivity of Jasperse *et al.* on natural LiF.

mation  $\Gamma(\nu)$  starts a little above  $\bar{\nu}_0$ . By 300 °K the isotopic absorption, which is temperature independent, will be small in comparison with the difference absorption below  $\bar{\nu}_0$ , but may be significant underneath the peak.

Second, it is clear from Figs. 6, 7, 10, and 11 that by 300 °K the three-phonon processes, occurring through the quartic anharmonicity, have to be considered.  $\Gamma(\bar{\nu})_{3-ph}$  will be fairly small and smooth, and will extend to higher wave numbers. Consequently its effect will be most noticeable near  $\bar{\nu}_0$  where  $\Gamma(\bar{\nu})_{2-ph}$  is, in the case of LiF at least, so low, and beyond the two-phonon limit. This is evident from  $\alpha$  measured beyond 1000  $\text{cm}^{-1}$  in Fig. 7 and from the 300 °K widths and heights of the  $\bar{\nu}_0$  resonance in  $\epsilon''$  and  $n$ , and from the peak reflectivity around  $\bar{\nu}_0$ . In fact the absorption beyond 1000  $\text{cm}^{-1}$  will be of the three-phonon-creation kind, which will be present even as the temperature,  $T$ , approaches zero, but which will, however, at "high" temperatures, tend towards a  $T^2$  dependence, compared with the limit of a linear  $T$  dependence for the two-phonon processes. At  $\bar{\nu}_0$  the three-phonon relaxation will involve the destruction of at least one phonon since the three-phonon-creation processes will almost certainly begin at higher energies than the two-phonon creation (summation) processes, which start above  $\bar{\nu}_0$ . Consequently there will be very little three-phonon relaxation of the TO resonance at 7.5 °K, and the only relaxation mechanisms will be the two-phonon difference and the isotope-induced one phonon.

Finally the features near 90 and 500  $\text{cm}^{-1}$  appear

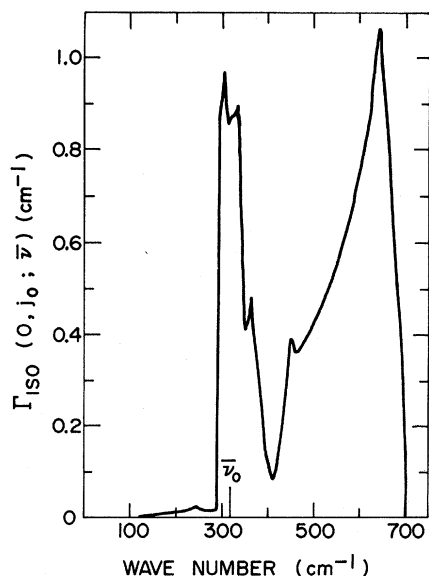


FIG. 12. The calculated temperature-independent damping of the transverse-optic mode of natural LiF at zero wave vector due to the isotope-induced one-phonon relaxation only, using 298 °K shell-model data.

to be too large (see  $\alpha$  in Fig. 8 and  $\epsilon''$  or  $n$  in Figs. 6 and 10.) This may be the result of inaccurate off-symmetry frequencies produced by the shell model, giving such large contributions near  $Q$  (see Table II), or it could possibly be due in some measure to eigenvector errors (see Ref. 22). A very probable cause is, however, the fact that in the coupling coefficient, all the two-body interactions, occurring through the Coulombic potential term have been assigned the same coupling characteristics as those calculated for nearest neighbors. This has overaccentuated the structure due to nearest-neighbor interactions. Next-nearest-neighbor coupling, etc., would occur strongly in different regions of the Brillouin zone. This may also explain why the predicted structure around 800  $\text{cm}^{-1}$  appears sharper than is seen experimentally.

It is hoped to present calculations and experimental data dealing with the second and third points above in the near future. Meanwhile, corrections due to the  $\text{Li}^6$  isotope (7.5 at. %) will now be presented so that the low-temperature data may be compared with the natural-LiF results.

#### IV. OPTICAL PROPERTIES OF NATURAL LiF AT 7.5 °K

Macdonald, Klein, and Martin<sup>23</sup> give an expression for the isotope-induced one-phonon absorption in alkali halides, which, however, does not remain finite through the TO resonance. The expression has therefore been used to yield an effective  $\Gamma(\bar{\nu})_{iso}$ , which can be added to the calculated  $\Gamma(\bar{\nu})_{2-ph}$ , and then through Eq. (20) the main resonance may be plotted as before, but with two independent relaxation mechanisms.

It was found that

$$\Gamma_{iso}(0, j_0; \bar{\nu}) = \frac{\pi \bar{\nu}^3 M^- \langle (\Delta M^+)^2 \rangle \rho^+(\bar{\nu})}{4 \bar{\nu}_0 (M^+)^2 (M^+ + M^-)}, \quad (32)$$

where  $\Delta M^+$  is the deviation at a particular site of the  $\text{Li}^+$  ion mass from the average  $M^+$ , and  $\rho^+(\bar{\nu})$  is the phonon density of states for the Li sublattice given by Eqs. (6) and (7) in Ref. 22.

The shell model was used to generate  $\rho^+(\bar{\nu})$ , which may be seen elsewhere.<sup>3,22</sup> It must be remembered, however, that although we are using these shell-model data and Eq. (32) to correct for isotope-induced absorption at 7.5 °K, the model actually generates data for isotopically pure  $\text{Li}^7\text{F}$  at 298 °K. The error in dispersion frequencies caused by 7.5 at. % of  $\text{Li}^6$  will, however, be small. The change in frequencies with temperature, however, is considerable and the measured value of  $\bar{\nu}_0(T)$  has had to be fed into the calculations. No attempt has been made to correct for the temperature variation of other frequencies, however, either in the two-phonon calculations of Sec. III or here in the Li-sublattice density of states  $\rho^+(\bar{\nu})$ .

The resulting  $\Gamma_{iso}(0, j_0; \bar{\nu})$  may be seen in Fig. 12,

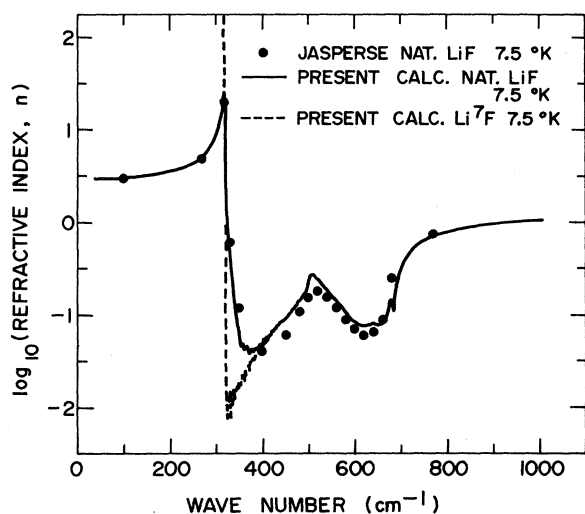


FIG. 13. The calculated refractive index  $n$  for natural LiF at 7.5 °K using one- and two-phonon independent relaxation, and for  $\text{Li}^7\text{F}$  at 7.5 °K using two-phonon relaxation only (see Fig. 10), with some of the natural LiF data points of Jasperse *et al.*

where the magnitude is obviously significant around  $\bar{\nu}_0$  but very small in comparison with  $\Gamma(\bar{\nu})_{2\text{-PH-SUM}}$ . From Figs. 1 and 2 it is clear that the isotopic one-phonon relaxation plays a major role in the height

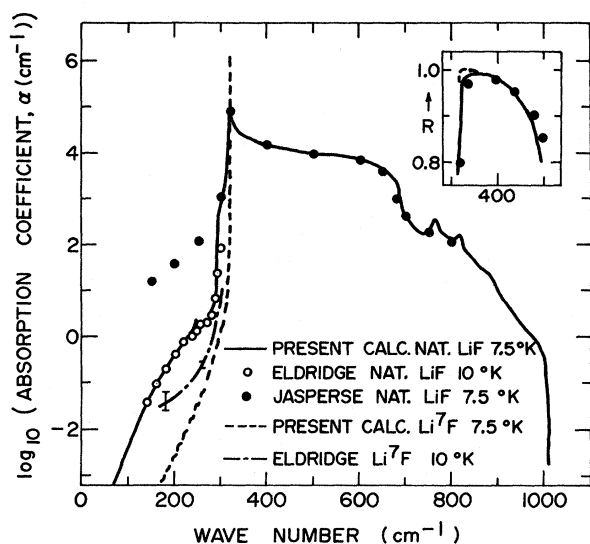


FIG. 14. The calculated absorption coefficient  $\alpha$  for natural LiF at 7.5 °K using one- and two-phonon independent relaxation, and for  $\text{Li}^7\text{F}$  at 7.5 °K using two-phonon relaxation only (see Fig. 9), with some of the natural LiF data points of Jasperse *et al.*, and the low-frequency transmission measurements of Eldridge (Ref. 22) with natural LiF and  $\text{Li}^7\text{F}$ . Inset is the calculated reflectivity  $R$  peak between 300 and 500  $\text{cm}^{-1}$ , calculated for  $\text{Li}^7\text{F}$  and natural LiF, both at 7.5 °K, with some of the natural LiF data points of Jasperse *et al.* at 7.5 °K (see Fig. 11).

and width of the TO resonance up to fairly high temperatures. By 300 °K  $\Gamma_{1\text{SO}}(\bar{\nu})$  is still approximately 50% of the size of  $\Gamma_{2\text{-PH-DIFF}}(\bar{\nu})$ . It is nevertheless not sufficient by itself to account for the peak-height discrepancies at 300 °K seen in Figs. 6 and 10, and the need for three-phonon terms remains. Both of these factors will also improve the 77 °K absorption coefficient agreement above 250  $\text{cm}^{-1}$  (see Fig. 8).

Not all of the 7.5 °K optical properties of Sec. III D need be recalculated with the inclusion of  $\Gamma_{1\text{SO}}(\bar{\nu})$ . It will be sufficient to show a real and an imaginary function together with the reflectivity peak. Figure 13 shows the real component of the refractive index  $n$ , calculated by including  $\Gamma_{1\text{SO}}(\bar{\nu})$  (natural LiF), together with the previous two-phonon-only calculated value seen in Fig. 10 ( $\text{Li}^7\text{F}$ ). The agreement with the data of Jasperse *et al.* of peak height at 300  $\text{cm}^{-1}$ , as well as the minimum between 300 and 400  $\text{cm}^{-1}$ , is excellent. As expected no alteration has occurred elsewhere. Figure 14 shows the absorption coefficient  $\alpha$  (obtained from the imaginary component of the refractive index) calculated for natural LiF and  $\text{Li}^7\text{F}$  at 7.5 °K. Together with the data of Jasperse *et al.*, the direct absorption measurements of Eldridge<sup>22</sup> below  $\bar{\nu}_0$  for natural LiF are included, as well as those already seen in Fig. 9. The agreement over the entire natural-LiF spectrum is satisfactory, especially the peak height. The low-energy points of Jasperse *et al.* are seen to be in error, due to the earlier-mentioned difficulty of obtaining the low imaginary values together with high real values from a power-reflectivity measurement.

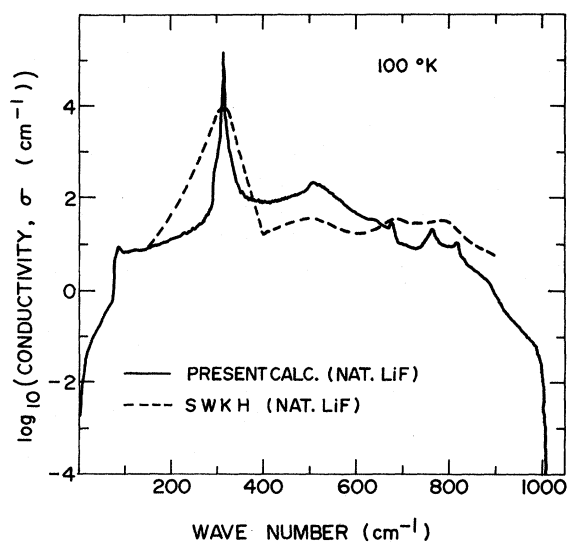


FIG. 15. The calculated conductivity  $\sigma$  for natural LiF at 100 °K using one- and two-phonon independent relaxation, with the experimental data from Smart, Wilkinson, Karo, and Hardy (Ref. 2).

As a demonstration of the preceding statement, the calculated reflectivity  $R$  for natural LiF is found to differ from that previously obtained only near the peak around  $335\text{ cm}^{-1}$  (see inset in Fig. 14). Thus the peak has been reduced from 100% at  $335\text{ cm}^{-1}$  to around 99% at  $360\text{ cm}^{-1}$ , somewhat closer to the measured values.

Finally, a calculation of the conductivity  $\sigma$  (equal to  $nk\bar{\nu}$ ) has been performed for natural LiF at  $100^\circ\text{K}$ . Although no more information is contained in  $\sigma$  than in  $\epsilon''$ , the calculation was performed in order to compare with the experimental results of  $\sigma$  presented by Smart, Wilkinson, Karo, and Hardy.<sup>2</sup> These data have been used for comparison earlier by this author<sup>1</sup> as well as by others.<sup>3</sup> Figure 15 shows the  $\sigma$  spectra in question. While there is general agreement about the positions of subsidiary maxima near 500, 680, and  $800\text{ cm}^{-1}$ , the intensity discrepancies are large. Upon reference to the original experimental work,<sup>24</sup> it may be seen that the experimental results are unreliable. The extinction coefficient  $k$  was obtained erroneously from thin-film transmission measurements, which yield knowledge of  $\epsilon''$  rather than  $k$ .<sup>25</sup> The refractive index was obtained from a Kramers-Kronig analysis of the measured reflectivity, which differed appreciably from reflectivity values reported elsewhere. The origin of the reported  $400\text{-cm}^{-1}$  feature, which was seen at a higher temperature, is therefore also questionable. It is thought that the calculated  $\sigma$  curve in Fig. 15 is reasonably accurate, therefore, for natural LiF. In the case of  $\text{Li}^7\text{F}$  at  $100^\circ\text{K}$ , the reststrahlen peak height is greater by a factor of 4 to 5 and the width is similarly decreased.

## V. CONCLUSION

Satisfactory agreement has been obtained both in intensity and structure between various experimental results of the optical properties of natural LiF and those calculated using third-order anharmonic coupling, shell-model frequency-dispersion data, and at low temperatures the isotope-induced one-phonon processes. The potential function employed has approximated the long-range coupling between all neighbors to give the correct order of magnitude in intensity, but has possibly overaccentuated the spectral features brought about by the nearest-neighbor coupling. Work is in progress<sup>26</sup> with KI (same structure) to check this point, and from a preliminary look at our room- and low-tempera-

ture data, together with the room-temperature data of Berg and Bell,<sup>5</sup> it appears to be a correct conclusion.

The calculated results at  $7.5^\circ\text{K}$  with two-phonon relaxation only, presented here, should be fairly valid for  $\text{Li}^7\text{F}$  (and indeed some agreement below  $\bar{\nu}_0$  is presented). The very high and sharp predicted TO resonance would be hard to measure, however, as the peak reflectivity approaches so close to 100%. Thin-film transmission measurements may be invalid since surface-relaxation processes may occur. The reason for the sharpness at low temperatures is coincidental inasmuch as the summation processes start at energies higher than  $\bar{\nu}_0$ . (It may be noted that the less accurate deformation-dipole data predicted summation processes at and below  $\bar{\nu}_0$ .) This leaves the difference processes (including the three-phonon mechanisms), which are low at  $\bar{\nu}_0$  in the first place, to decrease rapidly towards zero as the temperature is lowered. In KI, where the transverse-optic branch is higher with respect to the acoustic branches, two-phonon summation relaxation is always possible at  $2\bar{\nu}_0$  (as well as isotope one-phonon processes in the natural crystal once again). In CsI (which has a cubic structure), the same lack of summation processes under  $\bar{\nu}_0$  is again found,<sup>10</sup> and further the crystal has no natural isotopic impurities. The resonance should therefore also sharpen considerably with decreasing temperature. Much lower temperatures are required for the same effect, however, compared with LiF, because of the extreme disparity in hardness between the two crystals. Further details on the coupling responsible for the onset and limits of the two kinds of two-phonon relaxation processes will be presented in the near future.<sup>26</sup>

Further evidence has been found for the need to include the three-phonon processes resulting from quartic anharmonicity. Measurements at various temperatures are in progress<sup>10,26</sup> and various approximate methods of calculation will hopefully be shortly presented. Until such calculations are made and the accuracy of both experiments and theory is improved, the effect of neglecting the second-order electric moment will not be evident.

## ACKNOWLEDGMENT

The authors would like to thank Dr. G. Dolling for the building blocks of the shell-model program.

\*Work supported in part by Grant No. A5653 from the National Research Council of Canada and in part by Grant No. 9510-35 from the Defence Research Board of Canada.

<sup>1</sup>J. E. Eldridge, Phys. Rev. B **6**, 1510 (1972).

<sup>2</sup>C. Smart, G. P. Wilkinson, A. M. Karo, and J. R. Hardy, in *Lattice Dynamics*, edited by R. F. Wallis (Pergamon, New York,

1965), p. 387.

<sup>3</sup>G. Dolling, H. G. Smith, R. M. Nicklow, P. R. Vijayaraghavan, and M. K. Wilkinson, Phys. Rev. **168**, 970 (1968).

<sup>4</sup>K. W. Johnson and E. E. Bell, Phys. Rev. **187**, 1044 (1969).

<sup>5</sup>J. I. Berg and E. E. Bell, Phys. Rev. B **4**, 3572 (1971).

<sup>6</sup>W. Cochran, R. A. Cowley, G. Dolling, and M. M. Elcombe,

- Proc. R. Soc. A **293**, 433 (1966).
- <sup>7</sup>A. A. Maradudin and S. H. Vosko, Rev. Mod. Phys. **40**, 1 (1968).
- <sup>8</sup>R. F. Wallis and A. A. Maradudin, Phys. Rev. **125**, 1277 (1962).
- <sup>9</sup>R. A. Cowley, Adv. Phys. **12**, 421 (1963).
- <sup>10</sup>J. A. B. Beairsto and J. E. Eldridge, Can. J. Phys. (to be published).
- <sup>11</sup>M. Born and K. Huang, *Dynamical Theory of Crystal Lattices* (Clarendon, London, 1968), Appendix III.
- <sup>12</sup>Abraham Savitsky and Marcel J. E. Golay, Anal. Chem. **36**, 1627 (1964).
- <sup>13</sup>R. P. Lowndes and D. H. Martin, Proc. R. Soc. Lond. **308**, 473 (1969).
- <sup>14</sup>A. M. Karo and J. R. Hardy, Phys. Rev. **129**, 2024 (1963).
- <sup>15</sup>J. R. Jasperse, A. Kahan, and J. N. Plendl, Phys. Rev. **146**, 526 (1966).
- <sup>16</sup>D. Frohlich, Z. Phys. **169**, 114 (1962).
- <sup>17</sup>D. Frohlich, Z. Phys. **177**, 126 (1964).
- <sup>18</sup>M. Gottlieb, J. Opt. Soc. Am. **50**, 343 (1960).
- <sup>19</sup>H. W. Hohls, Ann. Phys. (N.Y.) **29**, 433 (1937).
- <sup>20</sup>M. Klier, Z. Phys. **150**, 49 (1958).
- <sup>21</sup>V. V. Mitskevich, Fiz. Tverd. Tela **4**, 3035 (1962) [Sov. Phys.-Solid State **4**, 2224 (1963)].
- <sup>22</sup>J. E. Eldridge, Phys. Rev. B **6**, 3128 (1972).
- <sup>23</sup>H. F. Macdonald, Miles V. Klein, and T. P. Martin, Phys. Rev. **177**, 1292 (1969).
- <sup>24</sup>C. Smart, Ph.D thesis (Kings College, University of London, 1962) (unpublished).
- <sup>25</sup>D. W. Berreman, Phys. Rev. **130**, 2193 (1963).
- <sup>26</sup>K. A. Kembry and J. E. Eldridge, Phys. Rev. B (to be published).

## Effect of Force-Constant Changes on the Lattice Specific Heat of $\text{KCl:Tl}$

M. D. Tiwari and Bal K. Agrawal

*Department of Physics, University of Allahabad, Allahabad 211002, India*

(Received 1 June 1972)

A detailed study of the effects of force-constant changes produced by noninteracting  $\text{Tl}^+$  impurity ions on the lattice specific heat of  $\text{KCl}$  has been made. Numerical computations have been performed for three impurity concentrations, 1, 3, and 5 mole % of  $\text{Tl}^+$ , and the results are compared with the experimental data of Karlsson. The effects of force-constant changes on the specific heat are seen to be quite large. The temperature dependence of the observed specific heat has been explained successfully by Green's-function theory in the temperature range 1–10°K. The force-constant change due to  $\text{Tl}^+$  in  $\text{KCl}$  is seen to be small and the impurity behaves essentially as a mass defect. Finally, the low-concentration theory is seen to be adequate for understanding the experimental results even at relatively higher concentration of impurities (5 mole % of  $\text{Tl}^+$ ) present in a crystal.

### I. INTRODUCTION

Quite striking changes in the phonon frequency spectrum of a crystal are obtained by introducing a finite concentration of impurities. The periodic symmetry of the crystal lattice is destroyed by the point defect. The normal modes of perfect crystal are thus modified. The modifications of the phonons are naturally large in the neighborhood of the defect. Essentially two new types of impurity modes may appear. The modes whose frequencies lie outside the range of those of the host crystal are called localized modes. This type of impurity mode is localized in the vicinity of the defect. The localized modes may appear owing to very light impurities such as  $U$  centers ( $\text{H}^-$ ) and/or owing to impurities strongly bound to the host lattice. Another type of impurity mode is a resonance mode. The frequencies of these modes lie in the range of the phonon frequencies of the perfect lattice and they are characterized by a considerable enhancement of the amplitude over a narrow range of frequencies. The resonance modes may occur owing to the presence of very heavy impurities and/or owing to impurities interacting very weakly with the host lattice. Recently, de-

tailed studies of impurity modes have been made by infrared-lattice-absorption,<sup>1-3</sup> inelastic-neutron-scattering,<sup>4-8</sup> and first-order Raman-scattering<sup>9,10</sup> experiments.

One of the most important properties of a crystal where the frequency spectrum plays a central role is the lattice specific heat. At low temperatures the high-frequency localized modes are not excited. At high temperatures a significant number of local modes are excited but all other phonons of the lattice are also excited. Thus the local modes will induce a relatively small change in the large total specific heat and the possibility of observing local modes in specific-heat measurements is very small. On the other hand, low-frequency resonance modes get excited even at low temperatures and can be observed in specific-heat experiments. Lehman and De Wames<sup>11</sup> and independently Kagan and Iosilevskii<sup>12</sup> have shown that the contribution of resonance modes to the lattice specific heat may be appreciable at low temperatures. Some numerical estimates for isotopic impurities have also been made by later groups of workers. Quite recently some combined experimental and theoretical studies<sup>13-15</sup> have been made for the temperature dependence of the lattice spe-